PROCEEDINGS OF SPIE

SPIEDigitalLibrary.org/conference-proceedings-of-spie

First results from the OGRESS sounding rocket payload

T. Rogers, T. Schultz, J. McCoy, D. Miles, J. Tutt, et al.

T. Rogers, T. Schultz, J. McCoy, D. Miles, J. Tutt, R. McEntaffer, "First results from the OGRESS sounding rocket payload," Proc. SPIE 9601, UV, X-Ray, and Gamma-Ray Space Instrumentation for Astronomy XIX, 960104 (18 September 2015); doi: 10.1117/12.2183237

SPIE.

Event: SPIE Optical Engineering + Applications, 2015, San Diego, California, United States

Downloaded From: https://www.spiedigitallibrary.org/conference-proceedings-of-spie on 9/14/2018 Terms of Use: https://www.spiedigitallibrary.org/terms-of-use

First results from the OGRESS sounding rocket payload

T. Rogers[1], T. Schultz[2], J. McCoy[2], D. Miles[2], J. Tutt[2], R. McEntaffer[2]

[1]University of Colorado, Center for Astrophysics and Space Astronomy, 593 UCB, Boulder, CO, USA, 80303
[2]University of Iowa, Van Allen Hall, Iowa City, IA, USA 52242

ABSTRACT

We present the first results from the Off-plane Grating Rocket for Extended Source Spectroscopy (OGRESS) sounding rocket payload based at the University of Iowa. OGRESS is designed to perform moderate resolution (R~10-40) spectroscopy of diffuse celestial x-ray sources between 0.3 – 1.2 keV. A wire grid focuser constrains light from diffuse sources into a converging beam that feeds an array of off-plane diffraction gratings. The spectrum is focused onto Gaseous Electron Multiplier (GEM) detectors. OGRESS launched on the morning of May 2, 2015 and collected data for ~5 minutes before returning via parachute. OGRESS observed the Cygnus Loop supernova remnant with the goal of obtaining the most accurate physical diagnostics thus far recorded. During the flight, OGRESS had an unexpectedly high count rate which manifested as a highly uniform signal across the active area of the detector, swamping the expected spectrum from Cygnus. Efforts are still in progress to identify the source of this uniform signal and to discover if a usable spectrum can be extracted from the raw flight data.

Keywords: x-ray spectroscopy, Cygnus Loop supernova remnant, sounding rocket, off-plane gratings, GEM detectors

1. INTRODUCTION

The soft x-ray sky is poorly understood on large angular scales. The workhorse satellites for x-ray astronomy, such as *Chandra* and *XMM-Newton*, achieve high spectral resolution based on their high quality focusing optics and their correspondingly narrow line-spread functions. Being slitless spectrographs, these instruments disperse a high-quality image of their target onto their focal planes and thus rely on the spatial resolution of their focusing optics to achieve their high spectral resolving powers when observing point sources[1]. Unfortunately, this technique is inadequate for diffuse sources due to their large sizes on the sky. When observing a diffuse source, the line-spread function is determined by the angular size of the target, rather than the spatial resolution of the telescope. As a result, the vast majority of spectral investigations have had to rely on the energy resolutions of the detectors aboard the *Chandra*, *XMM-Newton*, and *Suzaku* satellites. As these detectors were never intended to provide high energy resolution, this has resulted in a paucity of high resolution x-ray spectra for diffuse extended sources such as supernova remnants (SNRs), the galactic halo, the soft x-ray background, and solar wind charge exchange.

Our team has constructed an instrument designed to fill this gap in our data. The Off-plane Grating Rocket for Extended Source Spectroscopy (OGRESS) sounding rocket payload is capable of moderate spectral resolution ($E/\Delta E$ ~ 10-40) between 0.3 – 1.2 keV, while providing a Field Of View (FOV) large enough to fully encompass nearby diffuse sources (~10 deg^2). OGRESS's optical system is identical to that of CODEX[2], The Extended Off-plane Spectrometer[3,4,5] (EXOS), and the Cygnus X-ray Emission Spectroscopic Survey[6,7] (CyXESS). The payload consists of two nearly-identical spectrographs. Light is collected by passive focusers consisting of a stack of wire grids which sculpt a converging beam. Each focuser feeds into an array of off-plane gratings which disperse the light over ~2 meters onto Gaseous Electron Multiplier (GEM) detectors. The position of the detectors relative to the spectrum provides the only difference between the spectrographs. This instrument is capable of generating moderate-resolution spectra of large diffuse sources such as the Cygnus Loop and Vela SNRs.

The previous sounding rocket payloads, mentioned above, observed significantly higher signal than expected during their launches. This noise manifested as a highly uniform signal across the across the detector which swamped the

UV, X-Ray, and Gamma-Ray Space Instrumentation for Astronomy XIX, edited by Oswald H. Siegmund
Proc. of SPIE Vol. 9601, 960104 · © 2015 SPIE · CCC code: 0277-786X/15/$18 · doi: 10.1117/12.2183237

Downloaded From: https://www.spiedigitallibrary.org/conference-proceedings-of-spie on 9/14/2018
Terms of Use: https://www.spiedigitallibrary.org/terms-of-use

Figure 1: A single wire-grid plate bonded to its thick aluminum frame. In the zoomed image, we can see the individual wires and the slits between them.

expected signal from their science targets. As a result, OGRESS has been highly modified from previous designs in order to eliminate this previously unanticipated source of noise.

In section 2 of this paper, we will provide a description of the main components of the instrument. Section 3 will describe the problematic noise seen by previous payloads and explain the modifications made to OGRESS to increase throughput and reduce noise. Section 4 will explain OGRESS's flight plan and present our raw flight data. Section 5 will discuss the current status of our ongoing data analysis.

2. PAYLOAD DESIGN

2.1 Passive focusers

X-ray telescopes typically utilize grazing incidence mirrors to collect their light. These optics actively focus incoming light by changing its path via reflection. This can provide large collecting area and a narrow focus, but is typically heavy and prohibitively expensive for a sounding rocket budget. OGRESS uses a light-weight, inexpensive optical design which does not actively focus light, but rather destroys light which is not already coming to the desired focus. This is achieved with a series of 24 wire-grid plates stacked in sequence (see figure 1 for an image of a single plate). Moving from the front to the back of the focuser modules, the wires converge such that a sculpted beam is formed. Incident photons moving at undesired angles will eventually impact a wire and be destroyed, as shown in figure 2. Each plate has a total of 185 slits between the wires which sample adjacent areas of the sky. This leads to very low sensitivity for point sources which illuminate only a single slit in the focuser. However, this technique works quite well for large targets which fill the FOV and fully illuminate the beam of the telescope.

Figure 3 displays a view looking down the optical axis of the telescope. Distinct dark areas can be seen on each of the focuser modules. These dark areas correspond to the longest allowed path through the focusers from the angle of the camera. Note that the wire-grid plates only focus the light in a single dimension, resulting in long spectral lines seen at the focal plane, as shown in figure 2. This fact will require both the dispersive optics and our detectors to be large in order to capture all of the focused light.

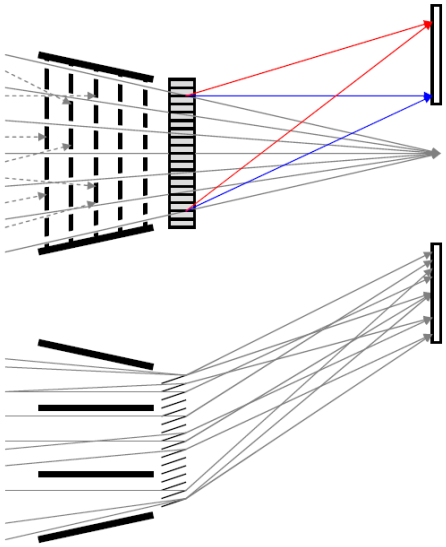

Figure 2: The top image shows the primary payload components (focuser, grating, detector) as seen looking down on the ruled surface of a grating. Nonconverging rays are vignetted by wires in the focuser. Rays that pass through would form a focus (gray lines), but are diffracted by the gratings and focused onto a detector. The bottom view is orthogonal to the top and looks along the direction of dispersion.

Figure 3: A view looking down the OGRESS passive focusers. To traverse the focusers, photon paths are limited to a specific angle, as can be seen in the dark line areas of each focuser. In this image, the star tracker's mass model is installed and the primary author can be seen reflected in the alignment flat.

Downloaded From: https://www.spiedigitallibrary.org/conference-proceedings-of-spie on 9/14/2018
Terms of Use: https://www.spiedigitallibrary.org/terms-of-use

2.2 Off-plane grating array

Light exiting the back of the passive focusers is diffracted by an array of reflection gratings in the off-plane mount[8]. Figure 4 shows a schematic of a single off-plane grating. In the off-plane configuration, light approaches the grating quasi-parallel to the grooves and diffracts in an arc. Off-plane gratings have been shown to achieve high reflection efficiencies at soft x-ray wavelengths[8], making them attractive for our applications.

We have chosen a graze angle of 4.4° for efficient reflection at low energies. The area of the focuser's final wire grid is 100 mm x 100 mm, thus the full grating array must fill this area to capture and disperse all of the light. Each grating is 104 mm x 20 mm, leading to a cross section of 1.53 mm x 104 mm to incident light (at 4.4° graze angle). In total, 67 gratings are required to fully capture the beam from the focusers. One of our two grating arrays is shown in figure 5.

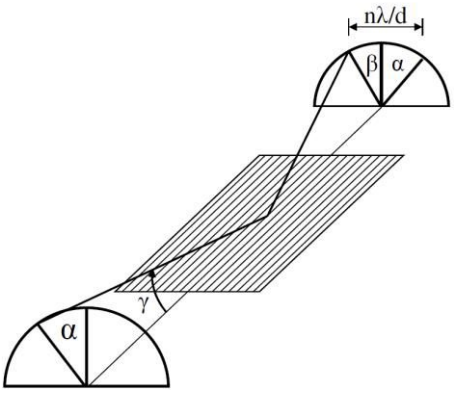

Figure 4: A schematic of a single off-plane grating. Light impacts the grating quasi-parallel to the grooves and diffracts in an arc.

Our gratings were holographically etched with a groove density of 5670 grooves/mm, allowing a spectral resolution of 10-40 across our bandpass when combined with the FWHM of the focuser modules. The gratings were replicated onto 125 µm electroformed nickel substrates made by Thin Metal Parts, Inc. Replication was done in an epoxy resist layer followed by a final nickel coating.

Maintaining flatness of the gratings is important for spectral quality. Therefore, the gratings are held in a Ti flexture mount which maintains 22 N of tension per grating. This has the added benefit of preventing the gratings from contacting one another during launch vibrations. These gratings have flown successfully on three previous missions[2,5,6], demonstrating the robustness of the design.

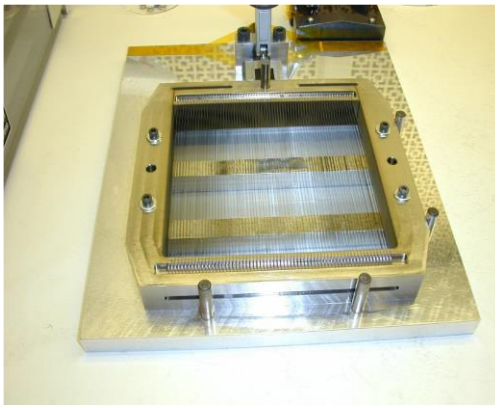

Figure 5: A grating array for one of the passive focusers. 67 thin gratings are held in a Ti tension mount to prevent them from contacting each other during launch vibrations.

2.3 Gaseous electron multipliers

Light from the gratings travels a distance of roughly 2 m before impacting the Gaseous Electron Multiplier (GEM) detectors. A basic diagram of a GEM detector is shown in figure 6. Photons pass through a thin polyimide window and ionize the Argon/CO_2 gas mixture inside the detector. The liberated electrons are accelerated by an electric field which is provided by a series of perforated copper plates. Each plate is held at a sequentially lower negative voltage. The electron shower is accelerated through the 70 µm holes in the plates and deposited onto a cross-delay-line resistive anode. In this way, GEMs are essentially proportional counters capable of spatial resolution. This spatial resolution is provided by the stack of copper plates and delay-line anode. GEMs have modest energy resolution, similar to typical proportional counters. This energy resolution cannot be used to make a high resolution spectrum, but it can be useful for removing high and low-energy noise from the

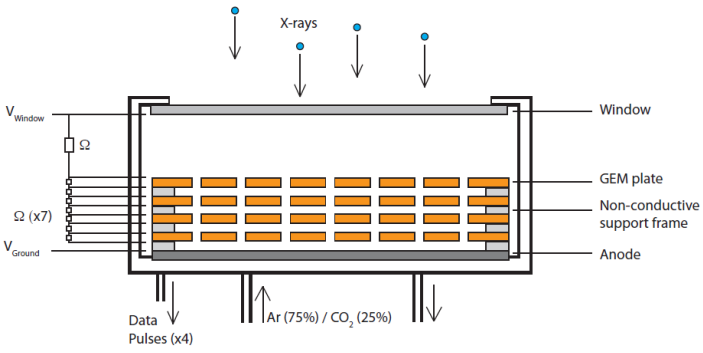

Figure 6: Schematic of a GEM detector. Light enters from above through a thin polyimide window and ionizes the argon gas. The window is held at roughly -3600 volts. The voltage is subsequently raised at the top and bottom of each copper GEM plate terminating at the grounded anode. The induced electric field accelerates liberated electrons and forms a cascade which is deposited on the anode.

Downloaded From: https://www.spiedigitallibrary.org/conference-proceedings-of-spie on 9/14/2018
Terms of Use: https://www.spiedigitallibrary.org/terms-of-use

collected spectra, as well as for separating different spectral orders, which will overlap on our detectors.

The advantages of GEM detectors are their high quantum efficiency to soft x-rays, low price, and their large size. As mentioned earlier, our focusers only act in a single dimension, leading to long spectral lines at the focal plane. Thus, the advantage of large detectors is two-fold. Along the direction of dispersion, detector size translates to observable bandpass, enabling us to collect a wide spectrum. Orthogonal to the direction of dispersion, detector size translates to effective area, since a larger detector will collect a larger portion of the long spectra lines. Our GEMs are 100 mm x 100 mm, the largest standard size available at the time of purchase.

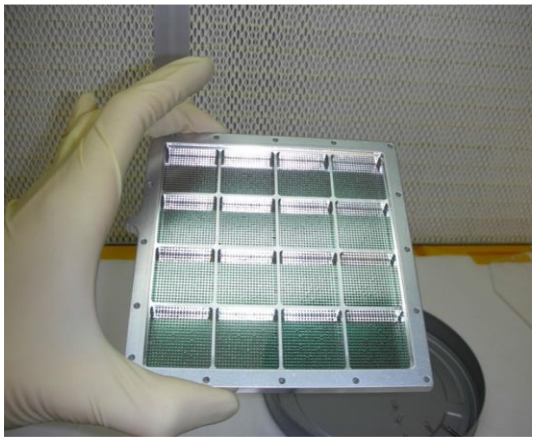

Figure 7: A detector window. The coarse aluminum grid is clearly visible. Looking closely, one can also see the fine mesh which provides additional support against the interior pressure of the detectors.

The detector windows must be designed to be thin enough to transmit soft X-rays, yet strong enough to withstand the ~ 1 atm pressure differential between the detector interior and the vacuum of space. Our GEM windows were manufactured by Luxel Corporation. They are ~5000 Å thick polyimide, coated with a 300 Å layer of carbon for conductivity, allowing the windows to be held at high voltage. To protect against tears, the windows are supported by a coarse aluminum grid, and a fine stainless steel mesh. This support structure allows a mechanical transmission of 57.8% and is displayed in figure 7.

2.4 Support electronics

In order to be telemetered to the ground, the raw asynchronous analog detector data must be digitized and synchronized. To accomplish this, each detector chain utilizes a series of preamps, time to digital converters, and Field Programmable Gate Array (FPGA)-based TeleMetry InterFace (TMIF) units. For a thorough description of OGRESS's support electronics, see McCoy et al. 2015[12].

3. PREVIOUS FLIGHT ISSUES

As mentioned above, OGRESS has heritage from several similar payloads launched by the University of Colorado. Data from the most recent of these flights showed that the previous payloads had observed an unidentified source of noise which manifested as a smooth distribution of counts over the active area of the detectors. The signal from this noise source was an order of magnitude stronger than the expected science signal and effectively reduced the Signal to Noise Ratio (S/N) such that the science target could not be detected[13]. In order to remove this unwanted noise, as well as to increase throughput and improve overall performance, substantial modifications were made to the OGRESS design.

3.1 Electronics

The electronics that OGRESS inherited were deemed to be outdated and a potential source for electronic noise. Thus, OGRESS's flight electronics were rebuilt from scratch with several substantial modifications. The final design is detailed in McCoy et al. 2015, but we will summarize the main changes here. In previous payloads, the raw data from the detectors was mixed together into a single analog channel prior to digitization. This resulted in confusion between the two detectors and 10-15% of the total counts would be assigned to the wrong detector in the data matrix[13]. For OGRESS, the detector chains were parallelized and were combined post-digitization, immediately preceding the TMIF system. As a result, OGRESS experienced no confusion between detectors. In addition to detector chain parallelization, OGRESS had many monitor signals added relative to previous payloads so that the general health and performance of the instrument could be monitored during flight. In addition to the raw detector data, OGRESS's telemetry stream included voltage and current monitors for all electrical components, as well as pressure data inside the payload, detectors, and gas reservoir.

3.2 Detector optimization

Optimizing the gain of our GEM detectors is extremely important, since soft x-rays have relatively low energy and thus produce few photoelectrons inside the detector gas chamber. Gain can be increased either by increasing the voltage between the copper plates or by decreasing the gas pressure inside the detector. Increasing the gain by either method results in an increasing risk of electrical arcing, so finding the ideal pressure and voltage is difficult. Previous

Downloaded From: https://www.spiedigitallibrary.org/conference-proceedings-of-spie on 9/14/2018
Terms of Use: https://www.spiedigitallibrary.org/terms-of-use

flights set the detectors to atmospheric pressure (the lowest pressure possible), and then optimized the voltage at ~ -4000 V. The detector pressure could not be set below atmosphere, because the windows are designed to hold a pressure difference in one direction. If the pressure within the detector falls below that of the outside, the detectors easily implode.

For OGRESS, we attached a vacuum system to the detector output gas lines to achieve pressures lower than atmosphere. To prevent detector implosion vacuum also had to be applied to the outside of the detector windows. Thus all detector testing was done under vacuum. By using pressures below atmosphere, we were able to find a truly optimal pressure-voltage combination, resulting in a higher gain than previous flights. OGRESS's detectors were optimized at ~10 psi and ~ -3500 V. The optimized pressure-voltage combination resulted in a reduced risk for window tears. It also made electrical arcing less of a problem by reducing their risk of occurrence as well as reducing their severity.

3.3 Ion repeller grid

The excess noise seen by previous flights was attributed to positively charged ions in the ionosphere being attracted to and eventually impacting the negatively charged detector windows[13]. Ions can produce counts in our detectors in two ways. First, if the ions are energetic enough to penetrate the detector window, they can impact and ionize the gas, beginning an electron cascade. Second, if the particles are highly ionized they can recombine with an electron when they impact the negatively charged window and emit an x-ray, producing a count in a more standard fashion.

Laboratory testing has shown that our GEM detectors see counts in the presence of an ion source. During post-flight testing of CODEX and pre-flight testing of OGRESS, a micro-ion gauge was used as an ion source to produce counts on the detectors. To solve the problem of ion noise, OGRESS flew a +100 V electrostatic ion repeller mesh to repel ≤ 100 eV ions. Electrons were not expected to be a potential noise source, as the detector windows carry a high negative charge, which should repel any thermal electrons within the payload. Laboratory testing showed that the strong contaminating signal resulting from the micro-ion gauge was effectively removed by turning on the ion repeller grids.

4. FLIGHT

4.1 Observing plan

Our observing plan was designed to ensure that we were aware of whether our instrument was functioning as intended. Although OGRESS was calibrated on the ground both before and after flight, we deemed it appropriate to perform in-flight calibrations, as flights of similar payloads have revealed significantly altered behavior during launch conditions.

Ensuring proper functionality of the detectors required that some time was dedicated to observation of a dark patch of sky. This allowed us to measure the difference between the signal from the natural sky background and Cygnus. We began by observing the off-target dark patch of sky, slewed onto Cygnus, and then repeated the cycle, as shown in figure 8. This was done to provide noise calibration near both 150 and 250km, in case our noise characteristics or sky background varied with altitude. For additional noise calibration, we kept the detectors turned on at the end of the flight for an additional 10 seconds after the shutter door closed. This was done to provide a true dark calibration of the detector noise in the absence of any signal from the sky.

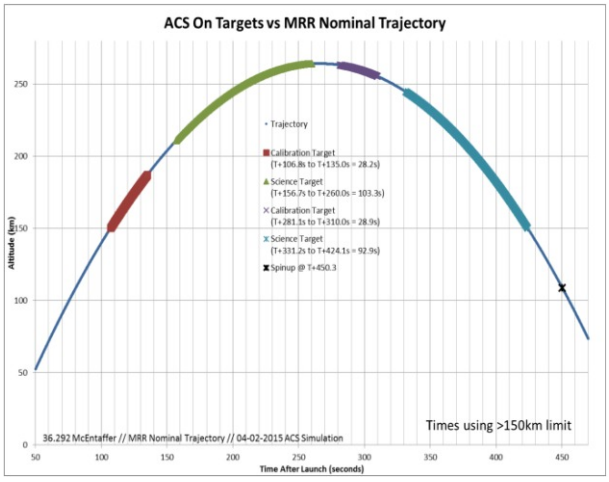

Figure 8: Plot of the targeting cadence during flight. Red and purple represent the dark calibration target. Green and blue represent the Cygnus Loop SNR. Not shown on the plot is the closing of the shutter door 10 seconds before turning off the detectors.

4.2 Flight data

OGRESS launched from White Sands Missile Range at ~2:30 am on Saturday May 2, 2015. As described above, the payload alternated between our calibration target and Cygnus for ~320 seconds. OGRESS received counts from our sky calibration source for ~60 seconds and from Cygnus for ~200 seconds. The remaining time was

Downloaded From: https://www.spiedigitallibrary.org/conference-proceedings-of-spie on 9/14/2018
Terms of Use: https://www.spiedigitallibrary.org/terms-of-use

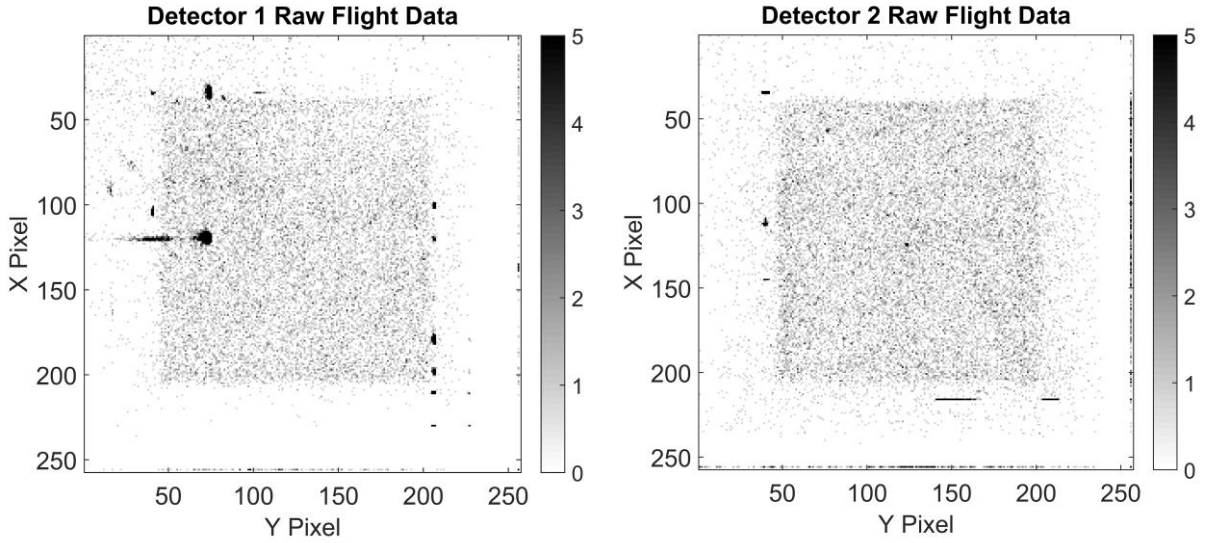

Figure 9: Plot of the raw flight data for both detectors. The majority of the counts fall into the active area of the detectors. Both detectors show stim pulses in locations consistent with laboratory testing. Detector 1 suffered from a hotspot (likely due to an imperfection in a copper plate) for the duration of the flight, but otherwise showed good performance.

lost during slew maneuvers. During flight, both detectors experienced separate minor arcing events which quickly stabilized and did not result in a change of performance.

The raw data from OGRESS's flight is shown in Figure 9. The raw data effectively sums the spectrum of our dark sky calibration target with that of the spectrum collected from Cygnus. Thus any spectral features shared between the sky background and Cygnus (such as a 0-order line) should be amplified. These images can be compared to Figure 10 which shows post-flight calibration data taken in the laboratory.

The flight data and calibration data share some basic similarities. In both pairs of images, the majority of the signal falls within a square region representing the physical, or active, area of the detector. Signal can fall outside this area in the presence of electronic noise, which can cause bits to be misanalysed. Both the flight data and calibration data show low levels of signal outside the active area due to position bits occasionally being misanalysed by our electronics.

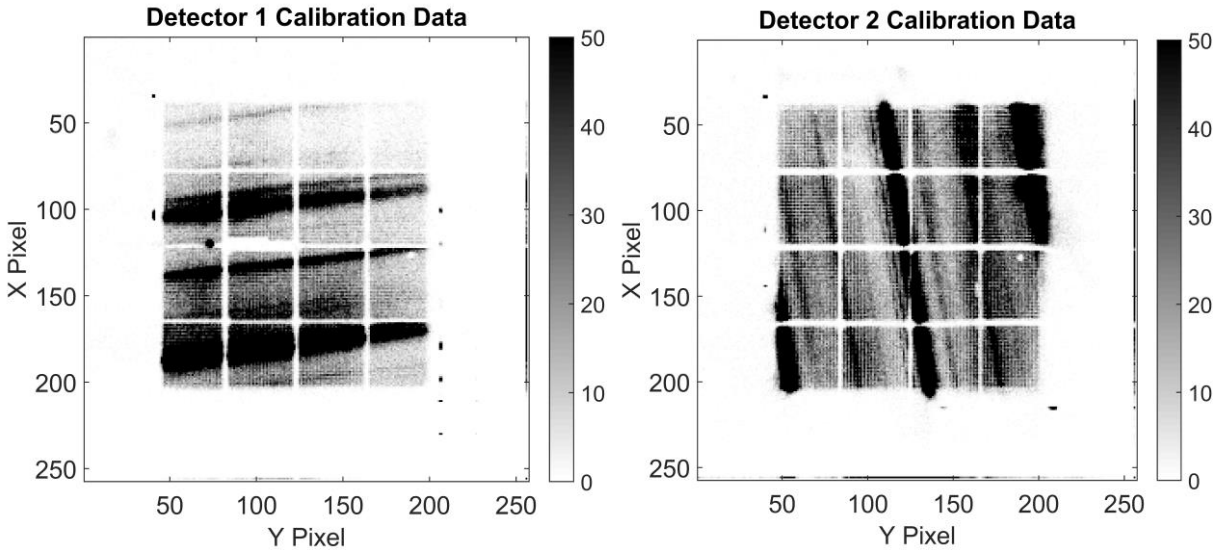

Figure 10: Plot of laboratory calibration data taken with an electron-impact x-ray lamp.

Downloaded From: https://www.spiedigitallibrary.org/conference-proceedings-of-spie on 9/14/2018
Terms of Use: https://www.spiedigitallibrary.org/terms-of-use

We also see strong signal in several points and streaks just outside the active area on the left and bottom edges of each image. These spots are intentionally created by sending electronic pulses into opposite ends of each detector anode. These "stim" pulses allow us to put a known signal through our detector chain giving us a clear indication of whether the detector electronics are functioning properly. Both our flight data and calibration data show stim pulses in the expected areas. Finally, Detector 1 has a hot spot apparent in both data sets, located on the left section of the active area. Persistent hot spots, such as this, are typically due to an imperfection in one of the GEM's copper plates. This can cause an easy path for electrons to flow to the anode, even in the absence of ionizing radiation.

Despite the similarities listed above, the differences between the two images are striking. This is not necessarily bad, as we do not expect the Cygnus Loop to look the same as our laboratory x-ray lamp. However, after accounting for differences in source brightness, exposure time, and intrinsic spectra, we do expect our flight data to look qualitatively similar to our calibration data. Several apparent issues with the flight data immediately present themselves.

1) We do not see obvious spectral features in our flight data, not even a 0-order line.
2) The flight data does not display the shadow features which are seen so prominently in the calibration data. These shadows are due to the aluminum grid and stainless steel mesh that were discussed in section 2.3.
3) The count rate seen by both detectors during flight is substantially higher than expected from previous measurements of Cygnus.

These issues suggest that OGRESS experienced an unanticipated source of noise that is much stronger than our science signal. This noise source appears to be producing a highly uniform distribution of counts across both detectors which is overwhelming the signal from Cygnus. There are many possibilities for our noise source which are currently being investigated in an attempt to qualitatively replicate our findings on the ground. We will discuss several possibilities below.

4.2.1 Electronic noise

Like other detectors, GEMs are sensitive to many varieties of noise arising from radio frequency interference, electrical arcing, noisy power supplies, improper grounding, and many other factors. Electronic noise can very often be distinguished from true signal because it does not always have to follow the physical constraints of the detector. In the case of our data, we can confidently rule out electronic noise as our primary source of contamination. As can be seen in figure 9, the majority of our signal falls within the active area of our detector, indicating that our observed signal originates outside the detector. We also see no difference between our stim pulses during flight and during ground testing. This indicates that electronic noise is not present.

4.2.2 Scattered light

It is possible that our high count rate is due to scattered light entering the detectors. The fact that there are no window grid or mesh shadows apparent in our flight data indicates that our source of noise is diffuse, and entering the detector from many different angles. Window grid shadows are only apparent when light strikes the detectors from a narrow range of angles. When light comes from all directions, the window grid shadows are eliminated entirely.

There are no direct paths for light to strike the detectors. The most direct route is through the focusing optics which involves a single grazing bounce off the gratings. Any light entering the detectors from an alternate path must make at least several near-normal incidence reflections which will completely eliminate any scattered x-ray signal. We may, however, be susceptible to high levels of scattered ultraviolet light which can make many reflection easily. Ultraviolet light will not be able to ionize the gas inside our detectors, but it is possible that high-energy ultraviolet photons could liberate electrons from the top copper plate. This would require a high level of flux, as ultraviolet light traveling through the detector gas will be strongly attenuated. However, with a high enough number of photons, scattered ultraviolet light could potentially become a significant source of noise.

Scattered light can be confidently rejected as the dominant source of our noise thanks to our final dark calibration exposure. As mentioned above, our detectors remained active for 10 seconds after closing the shutter door. During this time, there was little or no decrease in the count rate seen by the detectors. Figure 11 shows the smoothed count rates of both detectors. Both detectors show a very minor decrease in count rate for the final 10 seconds of data. This suggests that the detectors did indeed see x-ray signal from Cygnus, and that this signal was removed after closing the shutter door, as expected. Unfortunately, it cannot be said for certain whether this apparent drop in count rate is truly a result of our desired x-ray signal disappearing or whether it is simply a statistical fluctuation of the much stronger noise signal. It is clear, however, that after closing the shutter door, our source of noise remained present. This indicates that our noise may

Downloaded From: https://www.spiedigitallibrary.org/conference-proceedings-of-spie on 9/14/2018
Terms of Use: https://www.spiedigitallibrary.org/terms-of-use

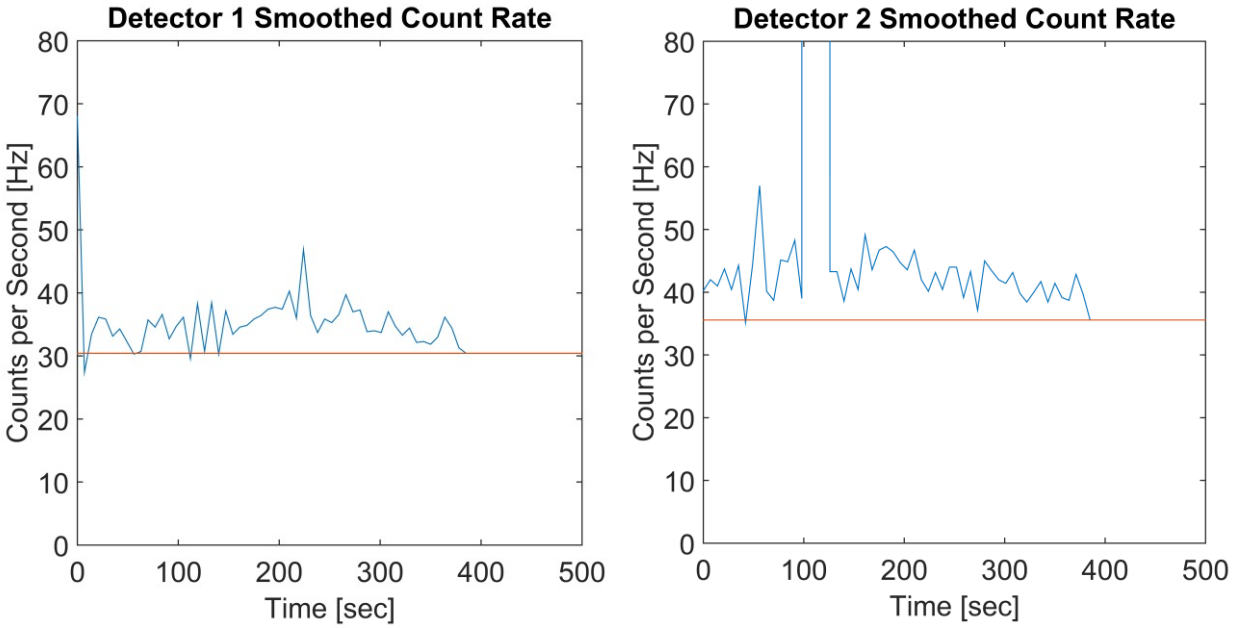

Figure 11: Plot of smoothed count rates inside the active area of each detector. Detector 1 shows a spike in count rate during turn-on and another during an arcing event at ~225 seconds. Detector 2 shows a spike in count rate prior to 100 seconds during an arcing event. Detector 2 also had a transitory hotspot for ~15 seconds that produced a massive spike in count rate while active. The times that this hotspot was active have been removed from plots of Detector 2 flight data. Both detectors show a slight drop in count rate at the end of the flight, indicating that scattered light is not our dominant source of noise, but that we may indeed be seeing signal from Cygnus and the sky.

be due to longer-lived particles which filled the payload after opening the shutter door and remained present inside the payload after the door closed. Charged particles in the atmosphere may be able to explain this phenomenon.

4.2.3 Charged particle impacts

As mentioned previously, the noise seen by previous payloads was thought to be due to positive ions impacting the detector windows. This scenario can now be ruled out due to the +100 V repeller grids which were placed in front of OGRESS's detectors. Thermal ions at 150-250 km will not have enough energy to penetrate a +100 V potential, even at the high end of the Maxwellian tail[14, 15]. High-energy charged particles can be ruled out as well, as they would require a direct or nearly direct path to the detectors which would result in a strong signal at the 0-order line, rather than a smooth distribution of counts over the detector faces.

4.2.4 Interior x-rays due to electrons

The currently favored explanation for the flight noise is that x-rays are being generated within the interior of the payload and impacting the detectors in the standard way. Since the x-rays are generated interior to the optics, the scenario would produce a uniform distribution of counts over the detector faces. There are two x-ray generation mechanisms that we are currently investigating. Both mechanisms rely on ionospheric electrons filling the payload and being accelerated by the strong electric field that is encountered close to the detector windows.

First, accelerated electrons will emit Bremsstrahlung radiation which can produce counts on the GEM detectors. Second, electrons which are accelerated by the strong interior electric fields will impact the aluminum interior of the payload and cause it to fluoresce x-rays. This second method is the same mechanism employed by our electron-impact calibration lamps that are used for laboratory testing. Both of these mechanisms – which can happen simultaneously – would produce a uniform distribution of counts across the face of our detectors. This signal would not necessarily dissipate within 10 seconds of closing the shutter door, as electrons can experience a large number of collisions before being absorbed.

Downloaded From: https://www.spiedigitallibrary.org/conference-proceedings-of-spie on 9/14/2018
Terms of Use: https://www.spiedigitallibrary.org/terms-of-use

Further support is lent to the interior fluorescence mechanism by Seward et al. 1973[16]. They investigated high-energy (~100 keV) electrons as a source of contamination for x-ray sounding rockets and tested several electrostatic and electromagnetic sweeping techniques in an attempt to remove these electrons from the optical path. Electrostatic sweepers were found to significantly increase the background count level when the applied voltage was set to ~280 V or above. The explanation was that at these voltages, thermal ionospheric electrons (distinct from the high energy electrons they were investigating) were being accelerated into the walls resulting in the generation of Carbon K-α x-rays. Inside OGRESS, electrons will first be attracted to the ion repeller grids (+100 V) and then will be repelled by the high voltage on the detector window (-3600 V). This will give them more than enough energy to generate Carbon or Aluminum K-α x-rays. It should be noted that the high energy electrons investigated by Seward et al. 1973[16] are not seen at WSMR and are therefore not considered to be a likely candidate for our noise source[17].

5. PRELIMINARY DATA ANALYSIS

At the time of writing, our data analysis is still very much ongoing, however we will present here the main finding of our analysis thus far. A basic histogram of our flight data (appropriately rotated based on the detectors' orientations relative to the spectral lines) is presented in figure 12. It is immediately apparent that we have no apparent spectral lines which can be confidently identified above the background noise level. The 0-order line should be our strongest spectral feature, regardless of the details of our spectrum. The position of 0-order has been marked at the center of Detector 2 (0-order does not fall onto Detector 1) and it is clear that the number of counts at this point are not noticeably higher than anywhere else. Significant lines expected from O VII have been marked on either side of 0-order. These lines are also not apparent above the background noise.

Although our raw flight data cannot provide a usable spectrum, we may still be able to remove some or all of the noise if we can distinguish it from our science data. We have reason to believe that our science data is, in fact, present beneath the noise. One reason is that after the shutter door closed our count rate lowered on both detectors by approximately the amount expected from Cygnus. This indicates that science data was successfully collected from Cygnus and can be utilized if it can be separated from the noise component. Figure 11, shown above, shows the smoothed count rate on both detectors throughout flight. The final seconds of flight (after shutter door close, but before HV off) have some of the lowest count rates seen throughout the flight, although there were several points with slightly lower count rates. This is not definitive, since the shift in count rate is not significantly higher than the natural variation

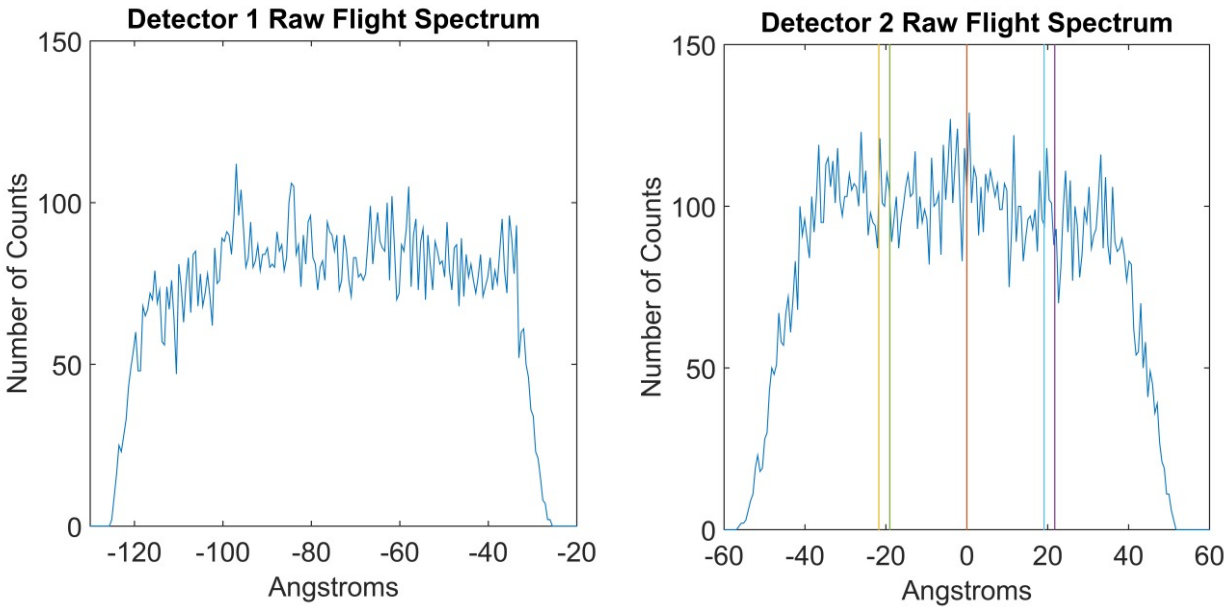

Figure 12: Plots of raw flight spectra on Detector 1 and Detector 2. Detector 2 has had locations marked where we expect prominent lines from O VII. The 0-order line location has also been noted at 0 Angstroms. None of these locations shows a noticeably larger number of counts than the background rate.

Downloaded From: https://www.spiedigitallibrary.org/conference-proceedings-of-spie on 9/14/2018
Terms of Use: https://www.spiedigitallibrary.org/terms-of-use

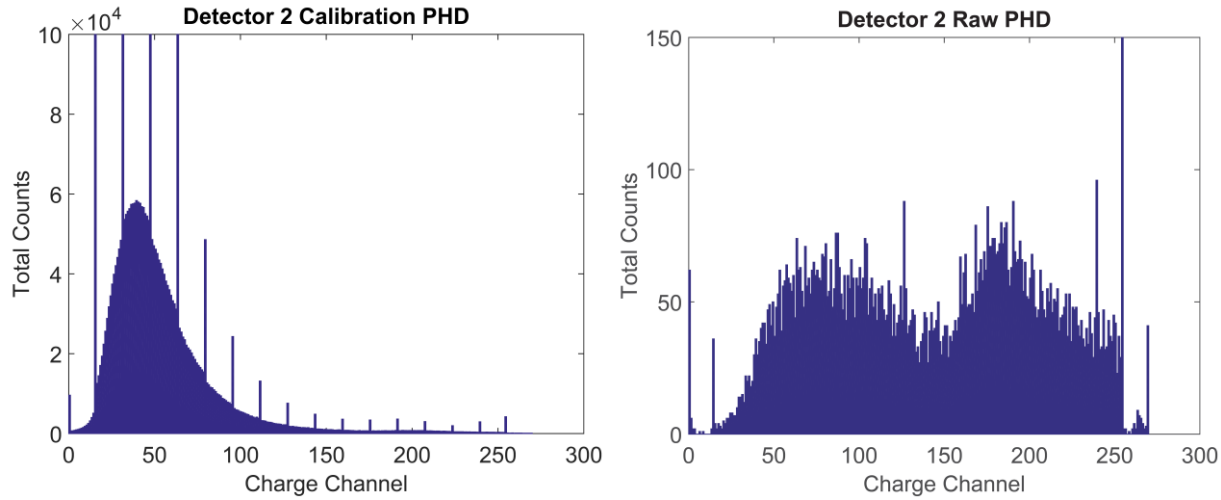

Figure 13: Plots of PH distributions of ground calibrations and flight data for Detector 2. During ground testing, Carbon and Oxygen K-α lines blend together. During the high count rates seen during laboratory calibrations, the low-significance bits are sometimes lost in the PH data, resulting in spikes every 8 channels. The flight data appears to have 2 distinct populations of counts, possibly indicating our science target and our noise source.

seen throughout the flight, but it is suggestive since the effect is seen on both detectors and is roughly the same number of counts we expect to receive from Cygnus.

The most reliable way to separate data from different sources is by Pulse Height (PH) of the counts. Every count registered by the detectors deposits a small pulse of charge onto the detector anode which is amplified and measured. The amount of charge deposited on the anode is correlated with photon energy, so our detectors have an intrinsic energy resolution which is potentially useful for separating overlapping spectral orders. This energy resolution can also be used to remove noise which has significantly different PH than the desired science data. Figure 13 displays the PH distribution of flight data within the active area of the 0-order detector (Detector 2). Laboratory calibration data

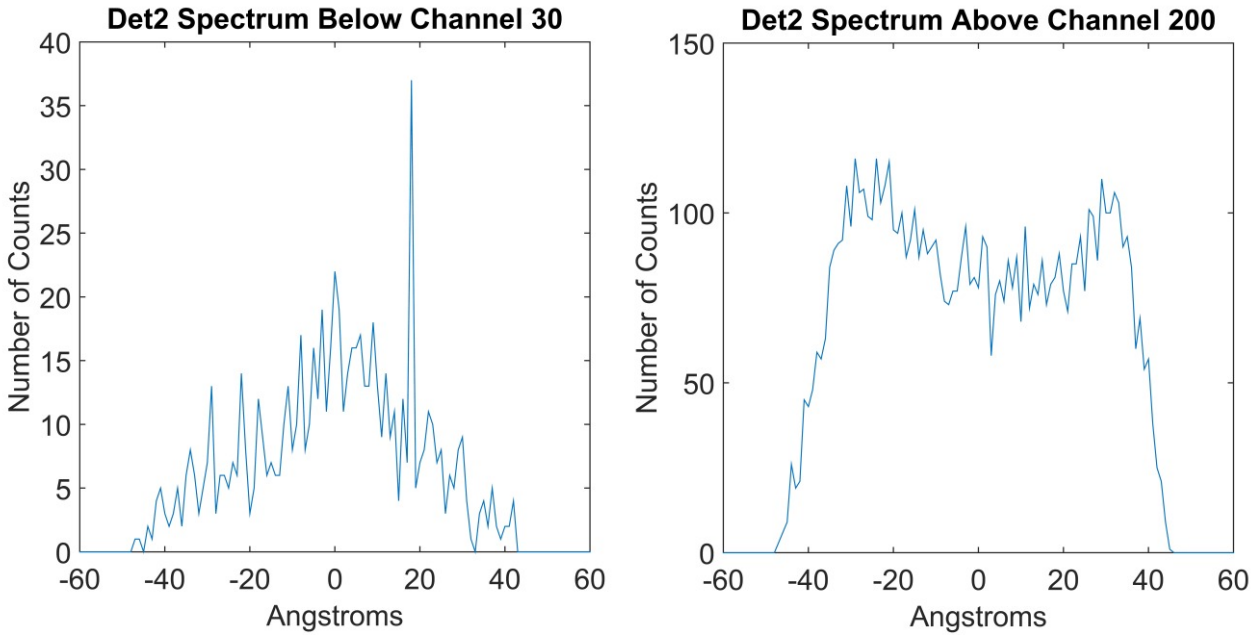

Figure 14: Plots of the flight spectrum on Detector 2 when only investigating counts which fall below charge channel 30 or above charge channel 200. These plots indicate that there may, in fact, be spectral variation across the face of the detector. Low-energy counts tend to fall near the center of the detector, as expected due to the 0-order line. High-energy counts tend to fall outside this area.

Downloaded From: https://www.spiedigitallibrary.org/conference-proceedings-of-spie on 9/14/2018
Terms of Use: https://www.spiedigitallibrary.org/terms-of-use

is also displayed showing a PH similar to what is expected from our science target. In the calibration data, the signal is dominated by Carbon and Oxygen K-α lines which blend together to make a smooth distribution with a high-energy tail. The flight data has notable features which are quite different from the calibration data. By eye, there appear to be two distinct populations of counts which follow different PH distributions. One distribution may be due to noise, and one may be due to our science data.

If the structure of the PH distribution is partly due to the spectral characteristics of our science data, then we expect the PH to vary over the face of the detector. Relatively low-energy counts should fall closer to the center of the detector due to the location of the 0-order line, and higher energy counts should fall outside this area. Figure 14 shows how the apparent spectrum across the detector face changes when we investigate only low-energy counts or only high-energy counts. Along the axis of dispersion, low-energy counts tend to fall in the center of the detector, and high-energy counts tend to fall closer to the edges of the detector. This is encouraging, since it suggests that we are beginning to find the spectral features of our spectrum that have been buried beneath the noise. It must be noted that this effect could also be due to a gain variation across the face of the detector, however we have several reasons to suspect that we are seeing a real spectral effect. First, a gain variation of this type is not theoretically expected in our detectors based on in-depth discussions with the manufacturers. Second, we have never seen this effect during laboratory testing. Finally, this effect is only present along the axis of dispersion. When looking perpendicular to this axis, no effect is present. More thorough laboratory testing is currently underway to more thoroughly characterize the gain variation across our detectors and to more definitively determine whether this effect is due to a gain variation or spectral characteristics.

5. SUMMARY

The OGRESS payload launched from White Sands Missile Range and targeted the Cygnus Loop supernova remnant. OGRESS utilizes a pair of wire-grid passive focusers and off-plane grating arrays to focus a spectrum onto two Gaseous Electron Multiplier detectors. Despite the modifications made based on previous flight problems, OGRESS observed a highly uniform background count rate which has swamped the science data, making extraction of the spectrum difficult. Despite the large amount of noise, there are indications that a usable spectrum is present within the flight data and may possibly be extracted for scientific analysis. Post-flight testing is currently underway to better characterize the detectors and enable the extraction of the highest quality spectrum possible.

ACKNOWLEDGEMENTS

The OGRESS payload and associated personnel are funded through NASA grants NNX13AD03G and NNX11AO10H.

REFERENCES

[1] Flanagan, K., Canizares, C., Dewey, D., Houck, J., Frederick, A., Schattenburg, M., Markert, T., David. D., "Chandra High-Resolution X-Ray Spectrum of Supernova Remnant 1E 0102.2-7219," ApJ, 605(1), 230-246 (2004)
[2] Zeiger, B., Shipley, A., Cash, W., Rogers, T., Schultz, R., McEntaffer, R., & Kaiser, M., "The CODEX sounding rocket payload," Proc. SPIE, 8076, 80760S,1-6 (2011)
[3] Oakley, P., McEntaffer, R., & Cash, W., "Soft X-ray Spectroscopy of the Cygnus Loop Supernova Remnant," ApJ, 766(1), 1-6 (2013)
[4] Oakley, P., McEntaffer, R., & Cash, W., "A suborbital payload for soft X-ray spectroscopy of extended sources," ExA, 31(1), 23-44 (2011)
[5] Oakley, P., Zeiger, B., Kaiser, M., Shipley, A., Cash, W., McEntaffer, R., Schultz, T., "Results from the Extended X-ray Off-plane Spectrometer (EXOS) sounding rocket payload," Proc. SPIE, 7732, 77321R, 1-6 (2010).
[6] McEntaffer, R., Cash, W., "Soft X-ray Spectroscopy of the Cygnus Loop Supernova Remnant," ApJ, 680(1), 328-335 (2008)
[7] McEntaffer, R., "Soft X-ray spectroscopy of the Cygnus Loop," PhDT, 0051(0606), 1-169 (2007).
[8] Cash, W., "X-ray optics. 2: A technique for high resolution spectroscopy," ApOpt, 30, 1749-1759 (1991)
[9] McEntaffer, R., DeRoo, C., Schultz, T., Gantner, B., Tutt, J., Holland, A., O'Dell, S., Gaskin, J., Kolodziejczak, J., Zhang, W., Chan, K., Biskach, M., McClelland, R., Iazikov, D., Wang, X., Koecher, L., "First results from a next-generation off-plane X-ray diffraction grating," ExA, Online First (2013)

Downloaded From: https://www.spiedigitallibrary.org/conference-proceedings-of-spie on 9/14/2018
Terms of Use: https://www.spiedigitallibrary.org/terms-of-use

[10] Katsuda, S., Tsunemi, H., Mori, K., Uchida, H., Kosugi, H., Kimura, M., Nakajima, H., Takakura, S., Petre, R., Hewitt, J., Yamaguchi, H., "Possible Charge-exchange X-ray Emission in the Cygnus Loop Detected with Suzaku," ApJ, 730(1), 1-15 (2011)
[11] McEntaffer, R., Brantseg, T., "*CHANDRA* Imaging and Spectroscopy of the Eastern XA Region of the Cygnus Loop Supernova Remnant," ApJ, 730(2), 1-10 (2011)
[12] McCoy, J., Schultz, T., Tutt, J., Rogers, T., Miles, D., McEntaffer, R., "A primer for telemetry interfacing in accordance with NASA standards using low cost FPGAs," JAI, Volume & pages to be determined (2015 expected)
[13] Zeiger, B., "Soft x-ray spectroscopy of the Vela supernova remnant," PhDT, Vol. 74-09(E), p.1-210 (2013)
[14] Kelley, M., [The Earth's Ionosphere: Plasma Physics and Electrondynamics], Academic Press, San Diego, 4-10 (1989)
[15] Bauer, S., Bourdeau, R., "Upper Atmosphere Temperatures Derived from Charged Particle Observation," JAS, Vol. 19, 218-225 (1962)
[16] Seward, F., Grader, R., Toor, A., Burginyon, G., Hill, R., "Electrons at low altitudes: a difficult background problem for soft x-ray astronomy," Proc of the Workshop on Electron Contamination in X-Ray Astronomy Experiments, Vol. 1, 1-25 (1973)
[17] Seward, F., "The Geographical Distribution of ~100-keV Electrons above the Earth's Atmosphere," Proc of the Workshop on Electron Contamination in X-Ray Astronomy Experiments, Vol. 1, 1-6 (1973)

Downloaded From: https://www.spiedigitallibrary.org/conference-proceedings-of-spie on 9/14/2018
Terms of Use: https://www.spiedigitallibrary.org/terms-of-use